Free-Space Time Domain Position Insensitive Technique for Simultaneous Measurement of Complex Permittivity and Thickness of Lossy Dielectric Samples

Zubair Akhter, *Student Member, IEEE*, and Mohammad Jaleel Akhtar, *Senior Member, IEEE*

***Abstract*— A novel time domain measurement technique is proposed to facilitate the simultaneous measurement of electrical properties (complex relative permittivity) and geometrical parameters (thickness) of the material under test (MUT). The overall process is noninvasive and noncontacting, which uses the measured scattering data of the MUT in the equivalent time domain or spatial domain. The effective time domain scattering data are employed to detect the primary and secondary peaks of the overall reflection and transmission coefficients. To this end, a novel algorithm is proposed to obtain the complex permittivity and thickness of the MUT in terms of extracted reflection and transmission power peaks. From the practical point of view, the main advantage of the proposed scheme is that one avoids the complicated calibration procedure normally required to define the reference plane. For increasing the accuracy of the overall reconstruction process, an automated optimization procedure based on parameter sensitivity analysis is proposed, which uses standard time gating procedure to implement the corresponding direct problem. The proposed technique is validated by extracting the relative permittivity, the dielectric loss (effective conductivity), and the thickness of various standard materials, such as polyethylene, Plexiglas, PVC, mortar, nylon, and so on, and comparing the extracted data with their values available in the literature.**

***Index Terms*— Dielectric material characterization, effective conductivity determination, Fourier transform, free-space measurement, material measurement, relative permittivity measurement, remote material characterization, time domain reflectometery, wave propagation, wideband.**

I. Introduction

In RECENT years, low cost, simple, and effective radio frequency (RF) dielectric testing technique of materials has been of much interest by researchers because of its importance in many practical situations. The material testing technique in the RF and microwave frequency band finds applications in food engineering, medical diagnostic, agriculture industry, civil engineering, and bioengineering [1]. Based on the nature of applications, the dielectric materials can be characterized using various methods satisfying the sample dimensions, the desired bandwidth (BW), and other essential requirements [2]. The microwave and RF material characterization methods can be broadly classified as resonant and nonresonant types. The resonant methods are found to have better sensitivity as compared with the nonresonant methods, but are usually suitable for low loss materials providing measurement at some specific frequency point [3]–[6]. On the other hand, the nonresonant methods can usually provide wideband RF characterization with good amount of accuracy, and are valid for materials with moderate losses [6]. The nonresonant methods, which mostly require measurements of reflection and transmission coefficient data, can be broadly classified into the guided transmission line [7]–[10], and the free-space method [11]–[24]. It may be noted that the free-space methods are quite convenient from the user point of view especially in the higher frequency region, as practically no sample preparation is required. The free-space methods can, in principle, be further classified under the frequency (spectral) domain and time (spatial) domains depending upon the methodology adopted for the reconstruction of dielectric properties in terms of measured data. The frequency domain free-space methods usually require the complicated calibration procedure, which sometimes becomes difficult due to nonavailability of accurate standards (conventional standard, i.e., open short through) for nonguided media.

The traditional time domain material testing methods are usually based on analytical formulations, and appear to provide a viable cost effective solution for the broadband microwave material characterization [7], [8], [25]. The main advantage of the time domain method is that it uses a simple calibration setup, and quite often, the involved calibration procedures used inherently in frequency domain approach can be avoided. This is facilitated with the help of standard time gating procedures, which can separate the scattering data of the test specimen from that of the background medium. In order to further ease the calibration procedure for time domain free-space measurements, various specialized techniques have been proposed in recent years to characterize the dielectric materials [12]–[24].

It should be noted than even the aforementioned specialized time domain techniques require an additional reference measurement for performing the calibration procedure. Most of these methods usually require the perfect electric conductor (PEC) as the standard reference material [17]–[24],

Manuscript received November 14, 2015; revised May 8, 2016; accepted May 31, 2016. Date of publication July 7, 2016; date of current version September 12, 2016. This work was supported by the Department of Science and Technology, New Delhi, India, under Grant SERB/EE/20130128. The Associate Editor coordinating the review process was Dr. Sasan Bakhtiari.

The authors are with the Department of Electrical Engineering, IIT Kanpur, Kanpur 208016, India (e-mail: zuakhter@iitk.ac.in).

Color versions of one or more of the figures in this paper are available online at http://ieeexplore.ieee.org.

Digital Object Identifier 10.1109/TIM.2016.2581398

and quite often a good conductor plate is being utilized in the place of PEC. However, the calibration procedure requiring the metal plate as a reference material might not be suitable for online monitoring of material properties due to several reasons. First, the metal plate should be placed at the reference plane of the material under test (MUT), which basically means that the test sample should be taken out of its place thus causing inconvenience under practical scenarios. Second, the calibration procedure then becomes position sensitive implying that the accuracy of the reconstruction will be affected if the MUT reference plane is shifted due to some reason from the reference plane. Finally, the overall reconstruction procedure might also be sensitive to the electrical properties of the reference material, such as its conductivity, surface roughness, and so on.

It is mainly due to above-mentioned reasons that an equivalent time domain or spatial domain method is proposed here to determine the dielectric properties and thickness of the test specimen, which does not require any specialized calibration scheme for measurements carried out in free space. In other words, the proposed method now does not depend upon the material properties of the reference, which might otherwise affect the overall accuracy of the reconstruction. In addition, the proposed scheme does not require any information about the thickness of the specimen in order to get electrical properties of the MUT. As a matter of fact, the thickness of the test sample is also determined using the proposed procedure in addition to the electrical properties using the proposed approach. To the best of our knowledge, such kind of equivalent time domain free-space method, where both the dielectric properties and the thickness of the test specimen are determined without requiring any reference calibration, has not been presented earlier in the literature. Hence, the proposed technique, in principle, is different from other time domain techniques presented earlier in the literature, which usually utilize a reference material measurement (PEC or highly conducting material) and provide only the electrical properties of the test specimen [18]–[25]. The closed form relations derived here relate the material properties with various reflection/transmission power peaks obtained after transforming the measured scattering parameters into equivalent time domain. In addition to the closed form analytical relationships, an automatic optimization algorithm is also proposed here, which directly compares the scattering coefficients of the test specimen in order to increase the overall accuracy of the reconstruction.

From the practical perspective, the proposed method employs a configuration where the MUT is placed in middle of two-antenna arrangement. Using this arrangement, the time corresponding to the first transmission gives an idea of possible occurrence of the first desired reflection from the test sample, and hence, the unwanted reflections from other sources, such as the antenna region, can be minimized. The problem of background reflection is removed with the help of absorbing boundary conditions by carrying out the measurement in the anechoic environment.

This paper is organized as follows. In Section II, the detailed description of the proposed theoretical algorithm to determine the dielectric properties in terms of the time domain scattering data is given. The numerical validation and the sensitivity analysis are presented in Section III with the help of the 3-D full wave simulator, the CST Microwave studio. The actual measurement configuration and performance assessments of proposed technique are conferred in Section IV, where the self-decisive optimization procedure is also described. The conclusions are stated in Section V.

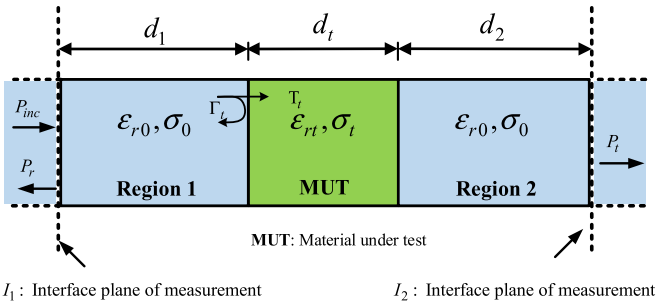

Fig. 1. Schematic representation of the microwave characterization of material.

II. Methodology

A. Problem Formulation

The MUT is assumed to be illuminated with the transverse electromagnetic (TEM) wave using the proposed microwave measurement configuration system, as shown in Fig. 1. The MUT with the relative permittivity (ε_{rt}), the effective electrical conductivity (σ_t), and the thickness (d_t) is placed in free space, such that the TEM wave is incident normally over the MUT. The term effective conductivity is mainly used here, a mathematical representation of the dielectric loss indicating that the constant conductivity model can be used to represent the dielectric losses. The effective conductivity is used quite often to represent effective dielectric losses due to static and alternating fields. However, it is to be noted here that many dielectric materials (glass and plastics) possess very low values of static conductivities, i.e., alternating conductivity dominate and a considerable amount of energy gets consumed when a dielectric is subjected to alternating fields as compared with its static counterpart [26]. Mathematically, the effective conductivity can be related with the effective tangent loss of the material using the following expression [26]:

$$\tan\delta_t \text{ (effective loss tangent)} = \frac{\sigma_t \text{ (effective conductivity)}}{2\pi f \varepsilon_0 \varepsilon_{rt}} \tag{1}$$

where $\varepsilon_0 = 8.854e-12$ is the free-space permittivity and f represents the frequency of operation. Meanwhile, the local voltage reflection coefficient of the test media (Γ_t) and the local voltage transmission coefficient of test media (T_t) with reference to background medium are also shown in Fig. 1. The configuration shown in Fig. 1 represents the most general scenario where the reflected power is measured in the background medium, having relative permittivity (ε_{r0}) and effective conductivity (σ_0), at a distance d_1 from the MUT. In a similar manner, the transmitted power is measured at the

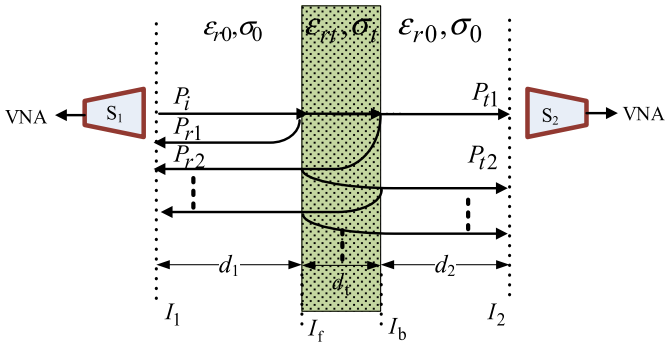

Fig. 2. Bounce diagram for the geometry shown in Fig. 1. A transient wave undergoes an infinite number of transmission and reflection at the interfaces.

opposite side of the interface at a distance d_2 from the MUT. The incident, reflected, and transmitted power components are represented as P_{inc}, P_r, and P_t, respectively. It is to be noted here that the background medium is considered to be lossless and dispersion-less throughout the formulation, which can represent the free space in most of the cases. In this paper, various primary and secondary reflection and transmission power quantities are directly taken from the vector network analyzer (VNA), which basically makes use of the complex scattering data (both magnitude and phase) to convert them into the equivalent time domain using the standard inverse fast Fourier transform (IFFT) routines. Hence, although the VNA makes use of both magnitude and phase information of the scattering data, the present formulation makes use of the power quantity only for determining the material properties and the thickness of the test specimen.

B. Algorithm Description

The typical reflection and the transmission bounce diagram in the time domain representing the reflected and transmitted powers from the test media are shown in Fig. 2, where S_1 and S_2 represent the antenna/sensor elements being responsible for transmission and reception of the RF power.

The reflection from or transmission through the test media (Ψ_i) can be expressed in the following generalized form:

$$\Psi_i = P_{Li} R_i A_i u(t-\tau_i) P_{\text{inc}}. \tag{2}$$

The term P_{Li} in the above expression describes the propagation condition, i.e., the path loss, which models the actual propagation condition in different wave propagation situations viz., the planar, the cylindrical, and the spherical [19]. Here, for the sake of simplicity, a plane EM wave incident normally over the test media is assumed. The term R_i considers various reflection and transmission factors when the wave propagates through the test media whereas A_i models the effective absorption through the test media. The term $u(t-\tau_i)$ is the unit step function, which signifies the received waveform with τ_i representing the arrival time of various reflection and transmission signals at sensor/antenna.

The first reflection sensed by the receiver, i.e., reflection from the front interface (I_f), observed by S_1 in Fig. 2 can be expressed as

$$P_{r1}(\varepsilon_{r0},\varepsilon_{rt},\sigma_0,\sigma_t,d_1,P_{\text{inc}}) = P_{L1}R_1A_1u(t-\tau_1)P_{\text{inc}} \tag{3}$$

where

$P_{L1}(d_1)$	two way path loss between the interface I_1 and I_f;
$R_1(\varepsilon_{r0},\varepsilon_{rt},\sigma_0,\sigma_t)$	local reflection from the interface I_f of MUT;
$\tau_1(\varepsilon_{r0},\sigma_0,d_1)$	time corresponding to primary reflection from interface I_f; $u(t)$ unit step function.

The second reflection, i.e., the reflection from the back interface of MUT (I_b), observed by TR_1, as shown in Fig. 2, can also be expressed as

$$P_{r2}(\varepsilon_{r0},\varepsilon_{rt},\sigma_0,\sigma_t,d_1,d_t,P_{\text{inc}}) = P_{L2}R_2A_2u(t-\tau_2)P_{\text{inc}} \tag{4}$$

where

$P_{L2}(d_1,d_t)$	two way path loss between the interface I_1 and interface I_b;
$R_2(\varepsilon_{r0},\varepsilon_{rt},\sigma_0,\sigma_t)$	two transmission (i.e., forward and reverse way) at the interface I_f and a reflection from interface I_b;
$A_2(\varepsilon_{rt},\sigma_t,d_t)$	material absorption;
$\tau_2(\varepsilon_{r0},\varepsilon_{rt},\sigma_0,\sigma_t,d_1,d_t)$	time corresponding to the second reflection.

In a similar manner, the primary and secondary transmitted power peaks can be expressed as

$$P_{t1}(\varepsilon_{r0},\varepsilon_{rt},\sigma_0,\sigma_t,d_1,d_t,d_2,P_{\text{inc}}) = P_{L3}R_3A_3u(t-\tau_3)P_{\text{inc}} \tag{5}$$

$$P_{t2}(\varepsilon_{r0},\varepsilon_{rt},\sigma_0,\sigma_t,d_1,d_t,d_2,P_{\text{inc}}) = P_{L4}R_4A_4u(t-\tau_4)P_{\text{inc}} \tag{6}$$

where

$P_{L3}(d_1,d_t,d_2)$ and $P_{L4}(d_1,d_t,d_2)$	path losses;
$R_3(\varepsilon_{r0},\varepsilon_{rt},\sigma_0,\sigma_t)$	transmission factor at the interface I_f and I_b successively;
$R_4(\varepsilon_{r0},\varepsilon_{rt},\sigma_0,\sigma_t)$	transmission factor at the interface I_f and I_b and reflection factor at the interface I_b and I_f, respectively;
$A_3(\varepsilon_{rt},\sigma_t,d_t)$ and $A_4(\varepsilon_{rt},\sigma_t,d_t)$	material absorption;
$\tau_3(\varepsilon_{r0},\varepsilon_{rt},\sigma_0,\sigma_t,d_1,d_t,d_2)$ and $\tau_4(\varepsilon_{r0},\varepsilon_{rt},\sigma_0,\sigma_t,d_1,d_t,d_2)$	time corresponding to the first and the second transmission, respectively.

The magnitude of reflection and transmission peaks described earlier in terms of incident power assuming a plane

wave propagation can also be written in the following form:

$$P_{r1} \cong |\Gamma_t|^2 P_{\text{inc}} \tag{7}$$

$$P_{r2} \cong |\Gamma_t|^2(1-|\Gamma_t|^2)^2 \exp\left(-2\sigma_t\eta_0\frac{1}{\sqrt{\varepsilon_{rt}}}d_t\right) P_{\text{inc}} \tag{8}$$

$$P_{t1} \cong (1-|\Gamma_t|^2)^2 \exp\left(-\sigma_t\eta_0\frac{1}{\sqrt{\varepsilon_{rt}}}d_t\right) P_{\text{inc}} \tag{9}$$

$$P_{t2} \cong (1-|\Gamma_t|^2)^2|\Gamma_t|^4 \exp\left(-3\sigma_t\eta_0\frac{1}{\sqrt{\varepsilon_{rt}}}d_t\right) P_{\text{inc}} \tag{10}$$

where $\eta_0 = 377\ \Omega$ (free-space intrinsic impedance) and P_{inc} is the reference incident power, as shown in Fig. 1. P_{r1} and P_{r2} represent the powers reflected from front and back interface of the test slab whereas P_{t1} and P_{t2} represent the direct path transmission and the consecutive transmission in time.

Equations (7)–(10) are taken as approximate in the sense that the term P_{Li} in all these equations is taken as 1 indicating a perfect plane wave or a TEM wave. Now, it is well known that the perfect plane wave concept is always an approximation, since under practical situation, the phase front over the full cross section of the test specimen might not represent an ideal plane. Equations (7)–(10) would be exact when the measurements are carried out in a guided medium representing a TEM wave.

From (7)–(10)

$$\sqrt{\frac{P_{r1}P_{t2}}{P_{t1}P_{r2}}} = \frac{|\Gamma_t|^2}{(1-|\Gamma_t|^2)} = k \tag{11}$$

where k is a constant, which can be determined using various reflection and transmission power peaks. Equation (11) can then be solved to determine the magnitude of the reflection coefficient with the constraint that $|\Gamma_t| < 1$.

Once the magnitude of the local reflection coefficient $|\Gamma_t|$ is determined, the relative permittivity and the thickness of test material can determined with the help of the following expression:

$$\varepsilon_{rt} = \left(\frac{1+|\Gamma_t|}{1-|\Gamma_t|}\right)^2 \tag{12}$$

$$d_t = \frac{c * \Delta\tau}{2\sqrt{\varepsilon_{rt}}} \tag{13}$$

where $\Delta\tau$ represents the time delay between P_{r1} and P_{r2}, and c is the velocity of EM wave in free space. After determining the permittivity and the thickness, the conductivity of the slab can be computed using

$$\sigma_t \cong \frac{1}{2d_t}\sqrt{\frac{\varepsilon_0\varepsilon_r}{\mu_0}}\ln\left(\frac{P_{r1}}{P_{r2}}(1-|\Gamma_t|^2)^2\right) \quad \text{or}$$
$$= \frac{1}{2d_t}\sqrt{\frac{\varepsilon_0\varepsilon_r}{\mu_0}}\ln\left(\frac{P_{t1}}{P_{t2}}|\Gamma_t|^4\right). \tag{14}$$

The derivation of (14) is facilitated with the help of (7)–(10).

The details of the proposed inversion algorithm can be explained using the following steps.

Step 1 (Optional): The measured scattering data (Fig. 1) are converted into equivalent time domain using the IFFT routines of the VNA.

Step 2: The second step involves the extraction of various parameters, such as P_{r1}, P_{r2}, P_{t1}, P_{t2}, and $\Delta\tau$, from the equivalent time domain representation of S-parameter data obtained in Step 1.

Step 3: Finally, with the help of (10)–(14), the values of the relative permittivity (ε_{rt}), the effective electrical conductivity (σ_t), and the thickness (d_t) of the test specimen are determined.

The proposed approach makes use of time corresponding to occurrence of the first transmission peak in order to identify various power terms required to reconstruct the dielectric properties and thickness of the test specimen. The problem of background reflections, if any, can be resolved with the help of absorbing boundaries by facilitating the measurements in the anechoic environment as discussed earlier. The time of occurrence of various power peaks can be verified by placing a metal plate at the material interface. It should be, however, noted that the metal plate is required here only for verification and not for any reference measurement.

C. Limitations on Bandwidth and Number of Frequency Samples

The BW (pulse rise time) and the number of frequency sample are very crucial parameters in order to get accurate reconstruction of the properties of test specimen using the proposed approach. The proposed technique makes use of various primary and secondary reflection/transmission peaks to determine the properties of MUT, and the time separation between these peaks directly depend on BW of the measured scattering data. Therefore, a compromise has to be made here between the thickness of MUT and BW of the scattering data such that various reflection and transmission peaks can be detected in the equivalent time domain. In other words, a minimum BW is required to resolve two adjacent interfaces (i.e., axial resolution) of the test specimen. The axial resolution δz in the range direction is determined approximately by the signal BW of the measured RF signal [27]

$$d_{\min} = \delta_z\ (\text{mm}) \approx \frac{c}{2\times \text{BW}} = \frac{10.71}{\sqrt{\varepsilon_{rt}}}. \tag{15}$$

Accordingly, a large signal BW results in an equivalent short pulse duration and hence provides a high range resolution. In most of the network analyzer, the number of points for the time domain representation is directly linked to the number of sample/points in frequency sweep (equal in most cases). Therefore, reducing the number of points in the frequency domain also results into less number of points in the time domain representation [28], which ultimately limits the ability of the procedure to detect and resolve various peaks in the delay domain. For example, if the spectral domain measurements are carried out over a BW, then the procedure cannot properly characterize a material having relative permittivity ε_{rt} if its thickness is below the minimum value given in (15).

The intermediate frequency (IF) BW is another important parameter in the VNA measurements, which basically corresponds to the BW of the IF filter. The smaller IF BW implies less broadband noise, which increases the effective dynamic range available for measurement. For lower permittivity samples, the magnitude of the reflection coefficient is low, and hence, the detection of various higher orders peaks,

TABLE I
RECONSTRUCTION OF MUT'S PARAMETERS

Materials ⇩	Material Properties @ CST library			Reconstructed (Proposed)			Error Analysis %		
Parameters ⇨	ε_{rt}	σ_t (S/m)	d_t (mm)	ε_{rt}	σ_t (S/m)	d_t (mm)	$\left\lvert\frac{\Delta\varepsilon_{rt}}{\varepsilon_{rt}}\right\rvert$	$\left\lvert\frac{\Delta\sigma_t}{\sigma_t}\right\rvert$	$\left\lvert\frac{\Delta d_t}{d_t}\right\rvert$
Teflon	2.10	2.33e-4	30	2.12	2.67e-4	30.248	0.95	14.5	0.82
Taconic HT(1.5)	2.35	3.26e-3	30	2.34	3.25e-3	30.374	0.42	0.30	1.24
Plexiglass	3.60	2.00e-2	30	3.58	1.99e-2	30.529	0.55	0.50	1.76
FR-4	4.30	5.98e-2	25	4.24	5.91e-2	25.448	1.39	1.17	1.79
CEM	4.40	7.34e-3	25	4.37	7.37e-3	25.377	0.68	0.40	1.50
Arlon-600	6.00	11.6e-3	25	6.02	11.5e-3	25.400	0.33	0.86	1.60
Berlliya	6.50	1.44e-3	25	6.48	1.40e-3	25.450	0.30	2.85	1.80
Silicon	11.9	2.50e-4	25	11.8	2.30e-4	25.386	0.84	8.00	1.54

such as P_{r2} and P_{t2}, becomes difficult. In order to detect these peaks, the reference noise label should be considerably low, which can be achieved by lowering the value of IF BW during measurement. It should, however, be mentioned that lowering the IF BW also slows the overall measurement process.

III. NUMERICAL VALIDATION

A. Simulation Procedure

Before testing the validity of the proposed technique against the experimental data, it is tested against the independent simulation data to closely observe the accuracy and range of validity of the proposed technique. For this purpose, the CST microwave studio is used to simulate the actual configuration, as shown in Fig. 1. The S-parameter is calculated for the frequency range of 26–40 GHz. In order to satisfy the plane wave condition, the boundary conditions are chosen, such that the structure supports the TEM mode of propagation as its dominant mode. In the present case, the parallel plate waveguide boundary condition (i.e., electric and magnetic boundaries along the mutually perpendicular faces) is used to facilitate the TEM mode of propagation. The waveguide ports are kept at a distance of $20 \times \lambda_{fc}$ from the MUT surface in both the directions, where λ_{fc} is the free-space wavelength at a center frequency of 33 GHz of band of interest. The thickness d_t of the MUT is ranging from 25–30 mm while the cross-sectional dimensions, i.e., length and width, are taken as $15 \times \lambda_{fc}$.

The itemized inversion algorithm presented in Section II has been applied on the simulated S-parameters. It is to be noted here that the number of frequency samples plays an important role as described earlier, and it is desirable to have more number of frequency samples for accurate peak detection. The number of frequency samples and the mesh cells considered in the current simulation are 10 000 and 2 862 250 (after symmetry plane reduction), respectively. For the validation of the proposed concept, a number of standard samples (with low-to-high dielectric contrasts with respect to free-space background) were used from the CST material library. The actual and the reconstructed relative permittivity, effective conductivity, and thickness of various standard materials are tabulated in Table I. The reconstructed material properties shown in Table I are obtained directly using the proposed set of closed form equations without any optimization.

The following observation can be made from Table I.

1) The proposed technique can estimate the relative permittivity of various standard samples having different dielectric contrasts with respect to the background media having a typical accuracy of 98% or more.
2) The thickness of the various test samples can also be accurately determined with a typical accuracy of 98% or more.
3) The proposed technique can also be used to evaluate the effective conductivity of various lossy dielectrics, and the typical accuracy can be quantified as follows.
   a) The lossy samples with $\sigma_t \simeq 10^{-3}$ or more can be characterized with a typical accuracy ranging from 99% to 97%.
   b) The dielectric samples with $\sigma_t \simeq 10^{-4}$ or less can be characterized with a typical accuracy ranging from 90% to 85%.

The sensitivity analysis has been done here for the MUT's parameter in order to find out the applicability of the proposed technique, and to obtain range of parameters values for which the optimum accuracy can be achieved.

B. Sensitivity and Error Analysis

In order to obtain the sensitivity of the proposed method, a detailed parametric analysis is carried out in this paper with respect to the electrical properties, i.e., the relative permittivity and the effective electrical conductivity. To this end, the test sample's electrical properties parametric variations against the measurable quantities, i.e., P_{r1}, P_{r2}, P_{t1}, P_{t2}, and $\Delta\tau$, are closely analyzed. The variations in the primary/secondary reflected and transmitted powers, i.e., P_{r1}, P_{t1}/P_{r2}, P_{t2}, with respect to the relative permittivity ε_{rt} of the MUT are presented in Fig. 3.

In Fig. 3, the associated scales of primary and secondary reflected and transmitted powers are represented along the left and the right sides of the y-axis, respectively. The following observations can be made from the detailed analysis.

1) The proposed algorithm is well suited for low as well as high dielectric contrast objects. However, the sensitivity is more for samples with low dielectric contrast as compared with those having higher dielectric contrasts.
2) The powers variation graph can play an important role during the optimization process (discussed

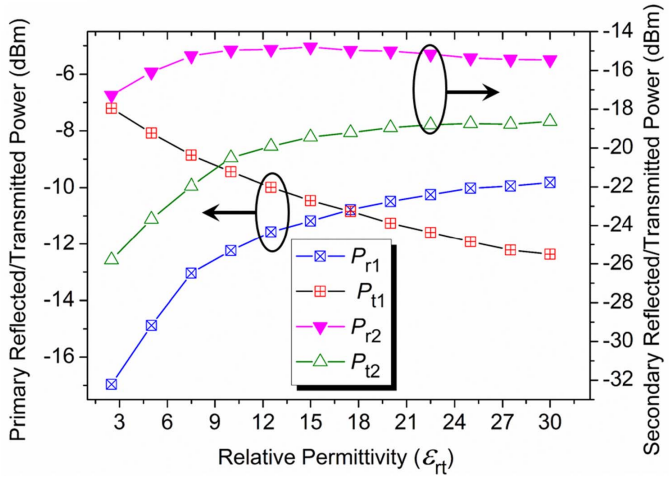

Fig. 3. Parametric analysis of reflected and transmitted powers with respect to relative permittivity of media under test as shown in the figure ($d_t = 15$ mm and $\sigma_t = 0$ S/m).

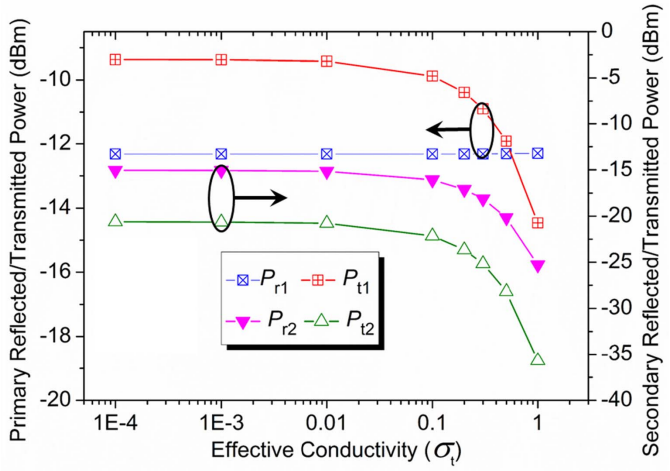

Fig. 4. Parametric analysis of reflected and transmitted powers with respect to effective conductivity of media under test ($d_t = 15$ mm and $\varepsilon_{rt} = 10$).

in Section IV) while updating the measurement variables, i.e., ε_{rt}, σ_t, and d_t.

The variations in primary/secondary reflected and transmitted powers, i.e., P_{r1}, P_{t1}/P_{r2}, P_{t2}, with respect to the effective conductivity σ_t of the MUT are presented in Fig. 4. In Fig. 4, the associated scales of primary and secondary reflected and transmitted power can be found at the left and the right y-axis, respectively. The following observations can be made from the outcome of this analysis.

1) The proposed technique is well suited for the characterization of lossy dielectrics with the effective conductivity ranging from 0.001 to 1.
2) The dynamic range of the proposed technique can also be made suitable for low loss dielectric materials provided that the sample thickness for these low loss samples is reasonably increased in order to observe a substantial change in the measured powers (reflected and transmitted) with respect to the dielectric loss.

It is to be noted that the power variation graphs, i.e., Figs. 3 and 4, providing the parametric variation behavior are quite important for the proposed optimization scheme presented later in this paper.

As discussed earlier, the BW plays an important role, since the probability of detection of higher order peaks directly depends on the BW. In case of low BW, or where the sample thickness is smaller than the minimum thickness required as mentioned in (15), the primary and secondary reflection and transmission peaks are merged together in time, thereby making the detection of all the four required peaks quite difficult. The quality of reconstruction near to this physical limit is analyzed here, so that the optimum thickness can be predicted in order to have good quality reconstruction. For this purpose, a simulation has been performed and the reconstructed values are plotted against the original values for different sample thicknesses. The outcome of this analysis can found in Fig. 5.

The minimum thickness required for a typical test sample (Arlon 600, $\varepsilon_{rt} = 6$, and $\sigma_t = 0.01168$) is roughly around 4.37 mm. When the thickness of the test sample is less than this limit, both the primary and secondary reflection and transmission peaks are merged together, giving rise to the dark zone. However, when the thickness of the test sample is increased from this limit, as shown in Fig. 5, the corresponding associated error becomes less.

IV. Measurement and Optimization

A. Free-Space Measurement

The proposed analytical technique requires the measurement of various reflection and transmission power peaks of the MUT using the free-space configuration shown in Fig. 6. The algorithm presented in Section III is then utilized to calculate the relative permittivity, the effective conductivity, and the thickness of the test sample. The actual measurement setup consists of two Ka band standard gain horn antennas, two Maury Microwave coaxial to waveguide adapters, and the Keysight VNA (E8361C). The measurement is carried out over a wide frequency range of 26.5–40 GHz. As stated earlier, the number of frequency data points is very crucial for the accurate determination of transmitted/reflected peaks. Therefore, the number of frequency data points and the IF BW are taken as $N_f = 6401$ and IFBW $= 30$ Hz for the entire measurement process. The transverse dimension of the test sample is taken to be larger than the antenna aperture in order to minimize the effect of the diffraction effects from the edges of the sample [11], [13]. In order to minimize the effect of edge diffraction, the distribution of the Poynting vector has been analyzed in past over the MUT's interface and criterion for transverse dimensions of sample has been made such that the normalized Poynting vector drops to -15 dB near the edges [15]. It is to be noted that if the lens-type focusing antennas are used for the free-space measurement and the test specimen is placed at the focus of both the antennas, then the cross-sectional dimensions of the test sample can be lower than the antenna foot print.

B. Measurement Results

In this section, the effective dielectric properties of some standards dielectric samples of different thicknesses are

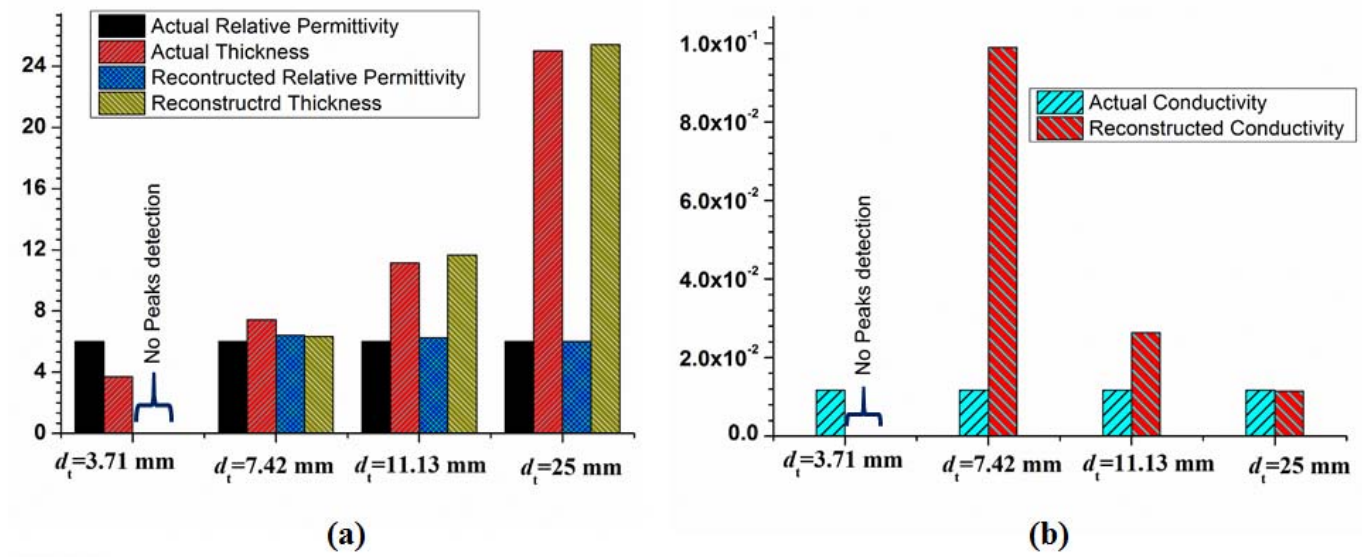

Fig. 5. Assessment of the proposed scheme for different sample thicknesses. (a) Comparison of actual and reconstructed values of relative permittivity and thickness. (b) Comparison of actual and reconstructed effective conductivity (test sample: Arlon 600, $\varepsilon_{rt} = 6$, and $\sigma_t = 0.01168$).

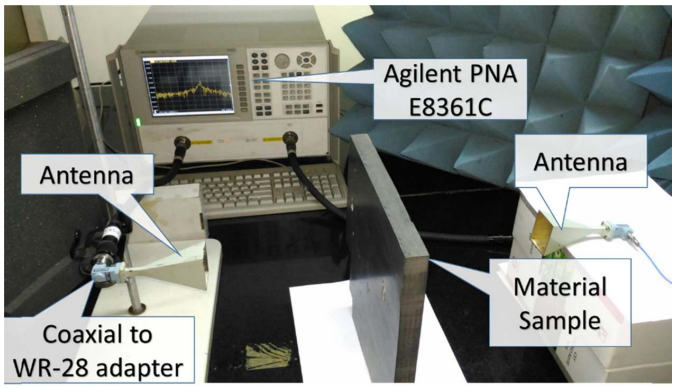

Fig. 6. Actual measurement setup.

obtained in order to validate the proposed approach. The samples are placed in between the two horn antennas, as shown in Fig. 6, such that the plane wave approximation can be made. It is to be noted here that the surface of the MUT should be preferably flat, which allows the EM wave to incident normally over the MUT surface. In the present case, the test samples are placed between the two antennas, which are separated by a distance of 70 cm.

The antennas are operating here in the frequency range of 26.5–40 GHz. The various power peaks are obtained using the IFFT routines of the VNA. The values of the relative permittivity, the effective conductivity, and the thicknesses of various samples are subsequently calculated with help of procedure explained earlier using (11)–(14). It is to be noted here that the dielectric properties of few reference samples considered here are not available in the literature for the frequency band of 26.5–40 GHz. In order to validate the measured data, the standards values are then taken from the adjacent reported frequency bands, assuming that the dielectric properties of these samples do not vary significantly with frequency.

The measurement is started by first considering a dielectric slab of Plexiglas (commonly referred as PMMA) with a dimension of $30 \times 30 \times 2.5$ cm^3, which is placed in between the transmitting and receiving antenna. Later, the a dielectric slab PVC and polyethylene of dimension $30 \times 30 \times 2.3$ cm^3 are placed between the two sets of antenna as described earlier. In a similar manner, various other dielectric samples, i.e., nylon, polypropylene, and polyacetal of dimensions $50 \times 50 \times 3$ cm^3 are being measured. A mortar sample with the dimension of $35 \times 35 \times 5$ cm^3 is also measured, and the values of the relative permittivity, thickness, and the effective conductivity are extracted using the proposed technique. It should be noted that the measurement of all the samples is carried out seven times, and accordingly the mean value and the standard deviation of the dielectric properties of each sample are listed in Table II.

C. Numerical Optimization Approach

The main aim of the analytical-based time domain approach proposed in Section III has been to determine the complex dielectric properties of the test specimen along with its thickness in terms of the equivalent time domain power quantities. The proposed approach does not directly require the complex scattering coefficients of the test specimen, and is practically adapted to free-space measurement without requiring any specific reference standards for calibration. The method works quite well for most of the standard dielectric samples as seen from validation using both the simulated and the experimental data. However, as mentioned in the previous part of this paper, various time domain power quantities in this paper are actually obtained from the IFFT of the measured spectral domain scattering coefficient data due to nonavailability of the required setup for direct time domain measurement. Hence, in situations where the complex scattering coefficients of the test sample are available, it looks useful to compare the scattering coefficients in the frequency domain in addition to comparing the time

TABLE II
MEASURED ASSESSMENT OF VARIOUS MUT'S PARAMETERS

Materials	d (mm)	Proposed method average @ f_c=33GHz			Reference value					|% error|		
		ε_{rt}	σ_t	d_t	ε_r'	ε_r''	$\tan\delta$	f(GHz) / Ref	σ_t^{Ref}	ε_{rt}	σ_t	d_t
Plexiglass	25	2.60±0.03	[1.18±0.02]e-2	25.57±0.26	2.67	-	1.24e-2	9.49/ [33]	1.7e-2	1.2	30	2.3
PVC	23	2.62±0.03	[7.60±0.04]e-3	23.79±0.29	2.59	-	1.02e-2	9.38/ [33]	1.3e-2	1.1	41	3.4
PETP	25	2.22±0.04	[4.31±0.04]e-3	26.01±0.32	2.18	-	6.5e-4	33.1/[31]	2.6e-3	1.8	65	4.0
Nylon	30	2.92±0.03	[6.53±0.02]e-2	31.24±0.25	2.99		1.8e-2	33/ [30]	9.8e-2	2.3	33	3.9
Polypropylene	30	2.23±0.04	[2.94±0.03]e-3	31.54±0.32	2.26 2.25		5.0e-4 1.5e-4	33/ [34] 35/ [29]	2.1e-3 6.5e-4	1.3	40	4.8
Mortar	50	6.98±0.08	0.6854±0.023	51.93±1.46	6.99	0.84	-	10/ [32]	0.467	0.1	46	3.8
Polyacetal	30	3.87±0.04	[1.54±0.02]e-2	31.53±0.35	-	-	-	-	-	-	-	-

domain power quantities to validate the reconstruction results. The goal of the optimization approach proposed in this section is to minimize the squared error between the measured and the simulated scattering coefficients in the frequency domain in order to obtain the dielectric properties and thickness of the test sample. Now, it is a well-known fact that for stable and fast convergence of any optimization approach and in order to avoid the local minima problem, very good starting values of the unknown parameters are required. In the present case, various parameters for the optimization approach are obtained using the proposed analytical approach expressed by a set of equations (12)–(14). It is worth mentioning here that most of the optimization approaches available in the literature provide only electrical properties of the test specimen [35], whereas the numerical optimization approach proposed in this section can reconstruct the thickness along with the electrical properties of the test specimen. In summary, it can be stated that the optimization approach proposed here in conjunction with the time domain approach described earlier can estimate dielectric properties of the test specimen along with its thickness provided that both the power scattering data and the reflection and transmission coefficients of test specimen are measured. The flowchart for the proposed optimization scheme is shown in Fig. 7.

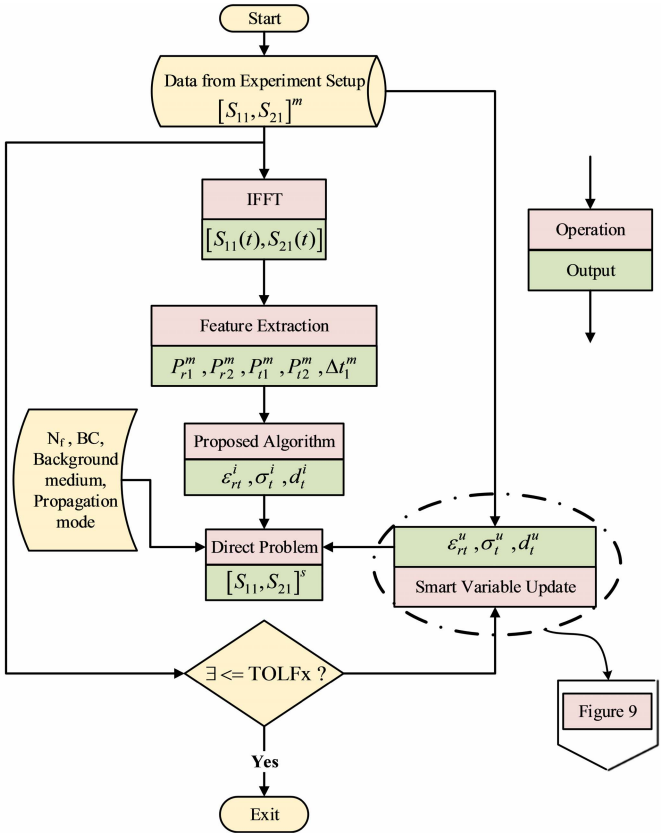

Fig. 7. Flowchart for the optimization of material parameter. Abbreviation—BC: boundary conditions, N_f: number of frequency samples, and TOLFx: tolerance function. Superscripts—m: measured, s: simulated, i: initial, and u: update. Subscripts—defined in the text.

Initially, the proposed analytical algorithm is used in conjunction with the directly measured scattering parameters in order to obtain initial values of the relative permittivity, the effective conductivity, and the thickness. The initial values obtained with the help of the proposed closed form equations are symbolically represented here as ε_{rt}^i, σ_t^i, and d_t^i, respectively. These initial values, i.e., ε_{rt}^i, σ_t^i, and d_t^i, are then used as input to the corresponding direct problem of the optimization scheme. The formulation of direct problem is done here using the standard T-matrix approach. The direct problem here is an independent MATLAB program that calculates the scattering parameters of the three layer problem, i.e., air–dielectric–air. It is to be noted here that the accuracy of the proposed optimization scheme strongly depends on the accurateness of direct problem formulation. It should be mentioned here that while utilizing the optimization procedure under practical scenario, the time gating function of the VNA has been used during the measurement procedure to collect the scattering data termed as $[S_{11}, S_{21}]^m$ in Fig. 7. The bandpass time gating is then performed, which considers the primary and secondary reflection/transmission peaks, i.e., P_{r1}, P_{t1}/P_{r2}, P_{t2}. Finally, with the deployment of time gating, the existing measurement state is converted into three layered media, i.e., air–MUT–air,

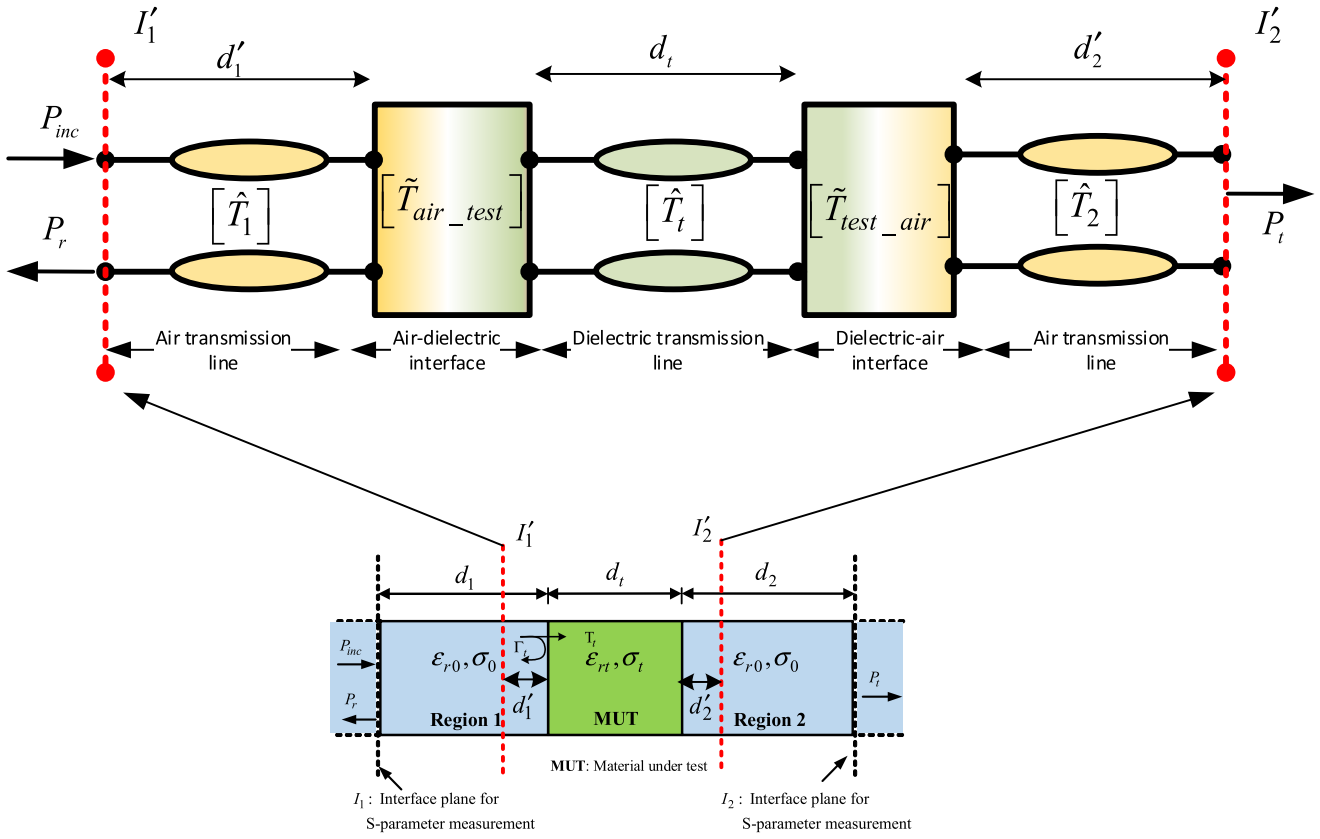

Fig. 8. Junction and transmission line representation of time gated domain of discontinuous media.

as shown in Fig. 8. Now, in order to implement the corresponding direct problem, the electrical and geometrical properties of each layer should be known in advance.

The initial values of these properties are obtained using the earlier proposed analytical time domain procedure. The procedure regarding the increment/decrement of the electrical and geometrical properties is given in Fig. 9. The important points regarding the proposed algorithm can be itemized as follows.

1) In order to apply the direct problem formulation over the reduced spatial domain, the parameters, such as d_1', d_2', ε_{r0}, σ_0, should first be determined using the earlier proposed analytical time domain procedure.
2) The decision regarding the increment/decrement of the electrical and geometrical properties is taken using a methodology given in Fig. 8.
3) The background medium in the present situation is considered to be air.
4) The thicknesses of background front and back layer d_1' and d_2' shown in Fig. 8 are calculated with the help of the following expressions:

$$d_1' = \frac{c \times \tau_1'}{2} \tag{16}$$

$$d_2' = \left(\tau_3' - \frac{\Delta\tau}{2}\right) \times c - d_1' \tag{17}$$

where c is the velocity of light in free space, $\Delta\tau_{\text{values}}$ represent the time separation between P_{r1} and P_{r2}, or P_{t1} and P_{t2}, and $\tau_1' = \tau_1 - \tau_{g\_\text{start}}$ and $\tau_3' = \tau_{g\_\text{stop}}$, where τ_{g_start} and τ_{g_stop} are the starting and stop time corresponding the bandpass gate function, respectively.

5) The S-parameter of the corresponding direct problem termed here as $[S_{11}, S_{21}]^s$ is then calculated with the help of T-matrix approach [35]. The number of frequency sample should be kept equal to the measured data samples so that they can be compared.
6) The calculated S-parameters are then compared with the measured time gated S-parameters and accordingly the objective function, i.e., the goal of the optimization, expressed as the mean square error between the measured (superscript m) and the simulated (superscript s) S-parameters, is defined using the following expression:

$$\exists = \sum_{i=1}^{N_f} \left\{ \begin{array}{l} \left(\left|\text{re}\left(S_{11}^m(i) - S_{11}^s(i)\right)\right|^2 \right. \\ \quad \left. + \left|\text{img}\left(S_{11}^m(i) - S_{11}^s(i)\right)\right|^2\right) \\ \quad + \left(\left|\text{re}\left(S_{21}^m(i) - S_{21}^s(i)\right)\right|^2 \right. \\ \quad \left. + \left|\text{img}\left(S_{21}^m(i) - S_{21}^s(i)\right)\right|^2\right) \end{array} \right\}$$

where N_f represents the number of frequency samples.

7) If the mean square error is in acceptable limit, the optimization routine will automatically stop. Otherwise, it will update the variable optimization variable, i.e., ε_{rt}^u, σ_t^u, and d_t^u. The smart variable update, a subroutine-based process, which is responsible for updating the optimization variables after each step, is shown in Fig. 8.

TABLE III
MEASURED ASSESSMENT OF VARIOUS OPTIMIZED MUT'S PARAMETERS

Materials	*Thickness* d (mm)	Proposed +Optimized			Standard values (literature)		Percentage error		
		ε_{rt}	σ_t	d_t	ε_{rt}	σ_t	$\left\lvert\frac{\Delta\varepsilon_{rt}}{\varepsilon_{rt}}\right\rvert$	$\left\lvert\frac{\Delta\sigma_t}{\sigma_t}\right\rvert$	$\left\lvert\frac{\Delta d_t}{d_t}\right\rvert$
Plexiglass	25	2.59	1.14e-2	25.56	2.67	1.7e-2	2.9	32	2.2
PVC	23	2.64	8.45e-3	23.46	2.59	1.3e-2	1.9	35	2.0
PETP	25	2.25	3.41e-3	25.32	2.18	2.6e-3	3.2	31	1.2
Mortar[#1]	50	6.93	6.74e-1	51.67	6.99	4.7e-1	0.8	43	3.3
Nylon	30	2.95	8.47e-2	30.51	2.99	9.8e-2	1.3	13	1.7
Polypropelene	30	2.24	2.56e-2	30.67	2.26	2.0e-3	0.8	28	2.2

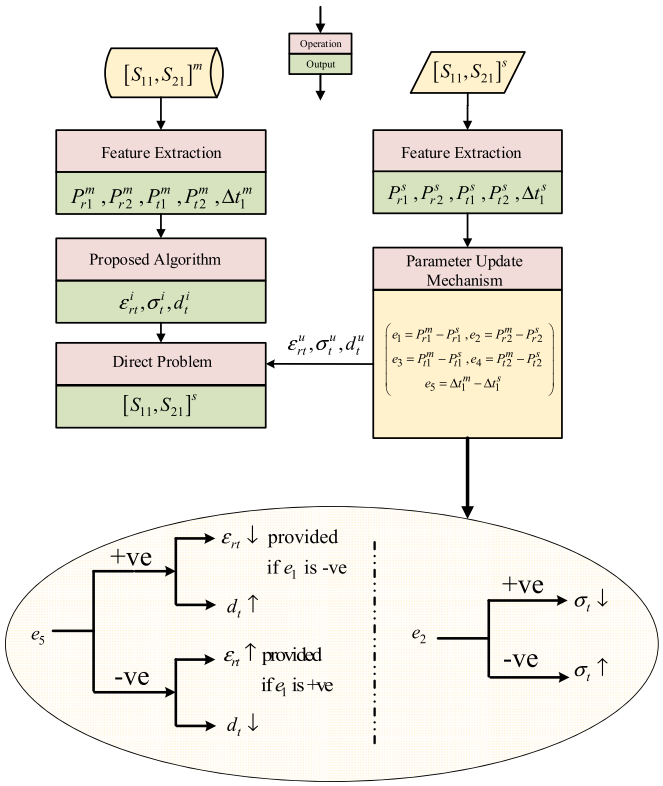

Fig. 9. Process diagram for the smart variable update with binary decision tree for updating the system parameter to obtain the optimum set of parameters.

The smart variable update subroutine utilizes different error terms, i.e., e_1 to e_5, as shown in Fig. 9. The values of different optimization variables (i.e., ε_{rt}^u, σ_t^u, and d_t^u) are then either incremented or decremented at each stage with respect to their previous values depending upon the sign of these error terms. The decision tree encircled shown in Fig. 9 utilizes here mainly the terms e_1, e_2, and e_5 to decide the convergence criterion and to arrive at the final solution. However, one can use other combinations of error terms, such as e_3, e_4, and e_5, as well to decide about the convergence criterion.

The reason for taking only three error terms to decide the convergence criterion is mainly due to the fact that they lead to fully independent sets of conditions. The following sets of observation obtained from the sensitivity analysis play a quite important role in decision making process for updating the optimization variables.

1) The calculated measured power components, i.e., P_{r1}^m and P_{r2}^m, are considered to be fixed during the whole optimization procedure.
2) There would be no change in the magnitude of P_{r1}^s, when effective conductivity σ_t is incremented or decremented. On the other hand, the magnitude of P_{r2}^s would be incremented if σ_t decreases and vice versa.
3) The error terms $e_1 = P_{r1}^m - P_{r1}^s$, $e_2 = P_{r2}^m - P_{r2}^s$, and $e_5 = \tau^m - \tau^s$ are considered here for optimization, where the objective here is to minimize the e_5 first.

The priority of minimizing error terms in the present situation is chosen using the following strategy.

1) First, the time difference between the primary and secondary reflections $\Delta\tau$ is examined, i.e., error term e_5 is selected first.
2) Based on the sign of the error term e_5, an appropriate path is chosen. For instance, if e_5 is positive, the sign of the error term e_1 is checked first, and ε_{rt} is either incremented (when e_1 is positive) or decremented (when e_1 is negative). It is to be noted here that the increment or decrement in ε_{rt} will improve both the error terms, i.e., e_1 and e_5.
3) Once, e_1 is minimized to a desired level of accuracy, then the role of d_t comes into existence. As shown in Fig. 8, d_t is either incremented (when e_5 is positive) or decremented (when e_5 is negative) until e_5 is minimized to the desired level, and accordingly, the final value of d_t is obtained. It is to be noted here that the value of error term e_1 does not vary during this update mechanism.
4) Finally, the error term e_2 is minimized by either incrementing the effective conductivity σ_t (when e_2 is negative) or by decrementing it (when e_2 is positive). The final value of the effective conductivity σ_t is accordingly obtained after the process is complete.

Table III shows the optimized value of the relative permittivity, the effective conductivity, and the thickness of some standard dielectric samples.

V. Conclusion

A novel time domain, calibration-independent microwave technique has been proposed here for the simultaneous extraction of the relative permittivity, the effective conductivity, and the thickness of the sample under investigation. The measurement has been performed for various standards (polyethylene, PVC, nylon, polypropylene, polyacetal, and Plexiglas) and laboratory made (mortar) samples, and it has been found that the measured results are in close agreement with the published data. The proposed inverse reconstruction procedure is expressed in terms of sets of equations representing a noniterative scheme, and, hence, looks appropriate for the real time application and can be envisaged for online monitoring of materials and processes. However, in order to increase the accuracy of the overall reconstruction under some situations, a special type of optimization scheme has also been presented in this paper. The proposed optimization scheme is quite time-effective, and provides stable solution by taking the initial values of the parameters from the proposed analytical algorithm. Based on the assessment of simulation and experiment, it is postulated that the proposed technique could estimate the relative permittivity, the dielectric loss, and the thickness of dielectric samples with low-to-moderate losses.

Acknowledgment

Z. Akhter would like to thank the reviewers for their comments, which clarified certain aspects and helped in improving the manuscript in current form. He would also like to thank S. P. Singh and A. K. Jha for their valuable discussion and suggestion.

References

[1] L. F. Chen, C. K. Ong, C. P. Neo, V. V. Varadan, and V. K. Varadan, *Microwave Electronics: Measurement and Materials Characterization*. West Sussex, U.K.: Wiley, 2004.

[2] "Basics of measuring the dielectric properties of materials," Agilent Technol., Santa Clara, CA, USA, Appl. Note 5989-2589EN, May 16, 2014.

[3] R. A. Waldron, "Perturbation theory of resonant cavities," *Proc. IEE C, Monographs*, vol. 107, no. 12, pp. 272–274, Sep. 1960.

[4] L. Chen, C. K. Ong, and B. T. G. Tan, "Amendment of cavity perturbation method for permittivity measurement of extremely low-loss dielectrics," *IEEE Trans. Instrum. Meas.*, vol. 48, no. 6, pp. 1031–1037, Dec. 1999.

[5] R. G. Carter, "Accuracy of microwave cavity perturbation measurements," *IEEE Trans. Microw. Theory Techn.*, vol. 49, no. 5, pp. 918–923, May 2001.

[6] J. Krupka, "Frequency domain complex permittivity measurements at microwave frequencies," *Meas. Sci. Techol.*, vol. 17, pp. R55–R70, Sep. 2005.

[7] A. M. Nicolson and G. F. Ross, "Measurement of the intrinsic properties of materials by time-domain techniques," *IEEE Trans. Instrum. Meas.*, vol. 19, no. 4, pp. 377–382, Nov. 1970.

[8] C. C. Courtney, "Time-domain measurement of the electromagnetic properties of materials," *IEEE Trans. Microw. Theory Techn.*, vol. 46, no. 5, pp. 517–522, May 1998.

[9] M. D. Deshpande, C. J. Reddy, P. I. Tiemsin, and R. Cravey, "A new approach to estimate complex permittivity of dielectric materials at microwave frequencies using waveguide measurements," *IEEE Trans. Microw. Theory Techn.*, vol. 45, no. 3, pp. 359–366, Mar. 1997.

[10] A. M. Paz, S. Trabelsi, S. O. Nelson, and E. Thorin, "Measurement of the dielectric properties of sawdust between 0.5 and 15 GHz," *IEEE Trans. Instrum. Meas.*, vol. 60, no. 10, pp. 3384–3390, Oct. 2011.

[11] D. K. Ghodgaonkar, V. V. Varadan, and V. K. Varadan, "A free-space method for measurement of dielectric constants and loss tangents at microwave frequencies," *IEEE Trans. Instrum. Meas.*, vol. 38, no. 3, pp. 789–793, Jun. 1989.

[12] K. Haddadi and T. Lasri, "Geometrical optics-based model for dielectric constant and loss tangent free-space measurement," *IEEE Trans. Instrum. Meas.*, vol. 63, no. 7, pp. 1818–1823, Jul. 2014.

[13] M. Bogosanovic, A. Al-Anbuky, and G. W. Emms, "Microwave nondestructive testing of wood anisotropy and scatter," *IEEE Sensors J.*, vol. 13, no. 1, pp. 306–313, Jan. 2013.

[14] K. Haddadi, M. M. Wang, O. Benzaim, D. Glay, and T. Lasri, "Contactless microwave technique based on a spread-loss model for dielectric materials characterization," *IEEE Microw. Wireless Compon. Lett.*, vol. 19, no. 1, pp. 33–35, Jan. 2009.

[15] C. Orlob, T. Reinecke, E. Denicke, B. Geck, and I. Rolfes, "Compact unfocused antenna setup for X-band free-space dielectric measurements based on line-network-network calibration method," *IEEE Trans. Instrum. Meas.*, vol. 62, no. 7, pp. 1982–1989, Jul. 2013.

[16] C. A. Grosvenor, R. T. Johnk, J. Baker-Jarvis, M. D. Janezic, and B. Riddle, "Time-domain free-field measurements of the relative permittivity of building materials," *IEEE Trans. Instrum. Meas.*, vol. 58, no. 7, pp. 2275–2282, Jul. 2009.

[17] S. Caorsi and M. Stasolla, "Characterization of lossy layers through monostatic radar measurements," in *Proc. 13th Medit. Microw. Symp. (MMS)*, Sep. 2013, pp. 1–4.

[18] B. K. Barman, Z. Akhter, M. J. Akhtar, and S. Mishra, "Microwave nondestructive testing of cement based materials," in *Proc. IEEE MTT-S Int. Microw. RF Conf. (IMaRC)*, Dec. 2013, pp. 1–3.

[19] S. Caorsi and M. Stasolla, "A layer stripping approach for EM reconstruction of stratified media," *IEEE Trans. Geosci. Remote Sens.*, vol. 52, no. 9, pp. 5855–5869, Sep. 2014.

[20] S. L. Gupta, Z. Akhter, M. Bhaskar, and M. J. Akhtar, "A novel half space time-domain measurement technique for one-dimensional microwave imaging," in *Proc. 83rd ARFTG Microw. Meas. Conf.*, Jun. 2014, pp. 1–4.

[21] S. L. Gupta, Z. Akhter, M. Bhaskar, and M. J. Akhtar, "Qualitative analysis of moisture content in cement based material using microwave non-destructive testing," in *Proc. IEEE Int. Symp. Antennas Propag. (APSURSI)*, Jul. 2014, pp. 924–925.

[22] K. K.-M. Chan, A. E.-C. Tan, L. Li, and K. Rambabu, "Material characterization of arbitrarily shaped dielectrics based on reflected pulse characteristics," *IEEE Trans. Microw. Theory Techn.*, vol. 63, no. 5, pp. 1700–1709, May 2015.

[23] Z. Akhter and M. J. Akhtar, "Time domain microwave technique for dielectric imaging of multi-layered media," *J. Electromagn. Waves Appl.*, vol. 29, no. 3, pp. 386–401, Jan. 2015.

[24] I. Vakili, L. Ohlsson, L. E. Wernersson, and M. Gustafsson, "Time-domain system for millimeter-wave material characterization," *IEEE Trans. Microw. Theory Techn.*, vol. 63, no. 9, pp. 2915–2922, Sep. 2015.

[25] K. Preis, O. Biro, P. Supancic, I. Ticar, and G. Matzenauer, "Time-domain analysis of quasistatic electric fields in media with frequency-dependent permittivity," *IEEE Trans. Magn.*, vol. 40, no. 2, pp. 1302–1305, Mar. 2004.

[26] C. A. Balanis, *Advanced Engineering Electromagnetics*. New Delhi, India: Wiley, 2013.

[27] M. I. Skolnik, *Introduction to Radar Systems*. London, U.K.: McGraw-Hill, 1980.

[28] M. Hiebel, *Fundamentals of Vector Network Analyzer*. Munich, Germany: Rodhe & Schwarz GmbH & Co. KG, 2005.

[29] M. N. Afsar, "Dielectric measurements of millimeter-wave materials," *IEEE Trans. Microw. Theory Techn.*, vol. 32, no. 12, pp. 1598–1609, Dec. 1984.

[30] Z. Abbas, R. D. Pollard, and R. W. Kelsall, "Complex permittivity measurements at Ka-band using rectangular dielectric waveguide," *IEEE Trans. Instrum. Meas.*, vol. 50, no. 5, pp. 1334–1342, Oct. 2001.

[31] V. N. Egorov, V. L. Masalov, Y. A. Nefyodov, A. F. Shevchun, and M. R. Trunin, "Measuring microwave properties of laminated dielectric substrates," *Rev. Sci. Instrum.*, vol. 75, no. 11, pp. 4423–4433, 2004.

[32] A. Hashemi, K. M. Donnell, R. Zoughi, M. C. L. Knapp, and K. E. Kurtis, "Microwave detection of carbonation in mortar using dielectric property characterization," in *Proc. IEEE Int. Instrum. Meas. Technol. Conf. (I2MTC)*, May 2014, pp. 216–220.

[33] A. K. Jha and M. J. Akhtar, "A generalized rectangular cavity approach for determination of complex permittivity of materials," *IEEE Trans. Instrum. Meas.*, vol. 63, no. 11, pp. 2632–2641, Nov. 2014.

[34] C. Yeh and F. I. Shimabukuro, "Circular dielectric waveguides," in *The Essence of Dielectric Waveguides*. Boston, MA, USA: Springer, 2008.

[35] M. J. Akhtar, L. E. Feher, and M. Thumm, "Noninvasive procedure for measuring the complex permittivity of resins, catalysts, and other liquids using a partially filled rectangular waveguide structure," *IEEE Trans. Microw. Theory Techn.*, vol. 57, no. 2, pp. 458–470, Feb. 2009.

Zubair Akhter (S'13) received the bachelor's degree in electronics and instrumentation engineering from Anand Engineering College Agra, Agra, India, in 2008, and the M.Tech. degree in RF and microwave engineering from IIT Roorkee, Roorkee, India, in 2011. He is currently pursuing the Ph.D. degree in electrical engineering with IIT Kanpur (IITK), Kanpur, India, with a focus on microwave imaging, material characterization, non-destructive testing of materials, through wall imaging and ultra-wide antennas for imaging applications.

He is currently involved in cost effective solutions for microwave imaging of concealed object, especially for homeland security applications. He has authored or co-authored over 20 scientific contributions published in peer-reviewed journals and various admired international conferences. His current research interests include developing a cost-effective microwave millimeter wave imaging setup for real-time imaging of concealed object where objects can be classified on the basis of their dielectric signatures rather that its physical parameters, such as shape, and size.

Mr. Akhter is the Founder and a Chair of the IEEE Antennas and Propagation Society Student Branch Chapter IITK, Uttar Pradesh Section, India.

Mohammad Jaleel Akhtar (S'99–M'03–SM'09) received the Ph.D. and Dr. Ing. degrees in electrical engineering from the Otto-von-Guericke University of Magdeburg, Magdeburg, Germany, in 2003.

He was a Scientist with the Central Electronics Engineering Research Institute, Pilani, India, from 1994 to 1997, where he was involved in the design and development of high power microwave tubes. From 2003 to 2009, he was a Post-Doctoral Research Scientist and a Project Leader with the Institute for Pulsed Power and Microwave Technology, Karlsruhe Institute of Technology, Karlsruhe, Germany, where he was involved in a number of projects in the field of microwave material processing. In 2009, he joined the Department of Electrical Engineering, IIT Kanpur, Kanpur, India, where he is currently an Associate Professor. He has authored two books, two book chapters, and has authored or co-authored over 100 papers in various peer-reviewed international journals and conference proceedings. He holds one patent on coplanar based RF sensors. His current research interests include RF, microwave and THz imaging, microwave nondestructive testing, RF sensors, functional materials, wideband electromagnetic absorbers, UWB antennas for imaging, and design of RF filters and components using the electromagnetic inverse scattering.

Dr. Akhtar is a fellow of the Institution of Electronics and Telecommunication Engineers, New Delhi, India, and a Life Member of the Indian Physics Association and the Indo-French Technical Association. He is a recipient of the CST University Publication Award in 2009 from the CST AG, Darmstadt, Germany. He served as a Chair of the IEEE Microwave Theory and Techniques Society-S Uttar Pradesh Chapter from 2013 to 2015, and the Vice-Chair of the IEEE Uttar Pradesh Section in 2015.